Supporting Information

Designing Kagome Lattice from Potassium Atoms on Phosphorus-Gold Surface Alloy

Shuo Sun,[1,2#] Songtao Zhao,[3#] Yong Zheng Luo,[1#] Xingyu Gu,[1] Xu Lian,[2] Anton Tadich,[5] Dong-Chen Qi,[6,7] Zhirui Ma,[2] Yue Zheng,[1] Chengding Gu,[2] Jia Lin Zhang,[1,2*] Zhenyu Li,[4*] Wei Chen[1,2,8,9*]

[1]Department of Physics, National University of Singapore, 2 Science Drive 3, 117542, Singapore

[2]Department of Chemistry, National University of Singapore, 3 Science Drive 3, 117543, Singapore

[3]College of Chemistry and Molecular Engineering, Qingdao University of Science and Technology, Qingdao, Shandong 266042, China

[4]Hefei National Laboratory for Physical Sciences at the Microscale, CAS Centre for Excellence and Synergetic Innovation Center of Quantum Information & Quantum Physics, University of Science and Technology of China, Hefei 260026, China

[5]Australian Synchrotron, 800 Blackburn Road, Clayton, Victoria 3168, Australia

[6]ARC Centre of Excellence in Future Low-Energy Electronics Technologies, School of Chemistry, Physics and Mechanical Engineering, Queensland University of Technology, Brisbane, Queensland 4001, Australia

[7]Centre of Materials Science, Queensland University of Technology, Brisbane, Queensland 4001, Australia

[8]Joint School of National University of Singapore and Tianjin University, International Campus of Tianjin University, Binhai New City, Fuzhou, 350207, China

[9]National University of Singapore (Suzhou) Research Institute, 377 Lin Quan Street, Suzhou Industrial Park, Jiangsu 215123, China

*To whom correspondence should be addressed: chmzhjl@nus.edu.sg (J.L.Z.), zyli@ustc.edu.cn (Z.L.) and phycw@nus.edu.sg (W.C.). #These authors contributed equally to this work.

1. Experimental Methods

1.1 Au(111) Preparation.

Clean Au(111) substrate was prepared by several cycles of Ar^+ sputtering (1.5 kV, 5×10^{-5} mbar) for 30 min and subsequent annealing at 500 °C for 30 min.

1.2 Two phases of BlueP-Au alloys Preparation.

The two phases of BlueP-Au alloys were prepared via molecular beam epitaxy (MBE) method in a UHV system with a base pressure of 2×10^{-10} mbar. Here, black phosphorus was used as the precursor, which was heated at 300 ℃. The P_2Au alloy was prepared by depositing phosphorus onto the clean Au(111) substrate held at 260 ℃ for 20min. Meanwhile, the P_4Au_3 alloy was prepared by depositing phosphorus onto the potassium functionalized Au(111) substrate held at 260 ℃ for 20min.

1.3 LT-STM Characterization.

In situ LT-STM experiments were performed in a custom-designed Unisoku system interfaced to a RHK controller with a base pressure of 2×10^{-10} mbar. All the measurements were carried out at 77 K using a Pt-Ir tip, with the bias voltage applied to the sample. The images were recorded under constant current mode.

1.4 XPS Measurements.

XPS data were acquired using a photon energy of 180 eV from the Soft X-ray Spectroscopy beamline at the Australian Synchrotron, using a SPECS Phoibos 150 hemispheric analyzer. Binding energies of all XPS spectra were calibrated using a clean gold foil in electrical contact with the samples. The base pressure of the analysis chamber is about 5×10^{-10} mbar.

1.5 DFT calculations.

Global structure search was performed using the stochastic surface walking (SSW)[1,2] algorithm implemented in the Large-scale Atomistic Simulation with neural alloy Potential (LASP)[3] code. Density functional theory (DFT) calculations were implemented in the Vienna *ab initio* simulation package (VASP).[4] The projector-augmented wave (PAW) method[5,6] was adopted to describe the electron-ion interaction, and Perdew-Burke-Ernzerhof (PBE)[7] functional was used to describe the exchange-correlation interaction. To account the long-range van der Waals (vdW) interaction, the semiempirical dispersion-corrected method of DFT-D3[8] was employed. The plane-wave cutoff energy was set to be 350 eV. The convergence criteria of total energy for electron self-consistency and force for geometry optimizations were 10^{-5} eV and -0.01 eV/Å, respectively. The bulk lattice constant of Au was scanned as 4.10 Å by using a Monkhorst-Pack k-point mesh[9] of ($21 \times 21 \times 21$). To study surface systems under the periodic boundary condition, a vacuum layer with a thickness at least 20 Å was inserted into the simulation cell. Au(111) surface slab was modeled with four layers of metal

atoms, and the bottom-layer atoms were kept fixed in their bulk positions during the geometry relaxation.

2. Supporting Figures, Notes and Table.

Figure S1 displays the LEED diffraction pattern for monolayer BlueP-Au alloy on Au(111). The red circles represent the underlying Au(111) substrate while the green circles represent the BlueP-Au alloy, which indicates the the lattice constant of BlueP-Au alloy is matched with the 5 × 5 supercell of Au(111).

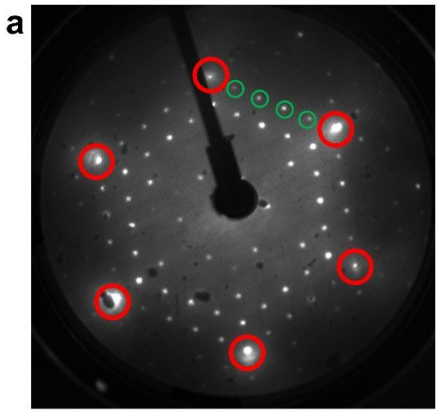

Figure S1. LEED diffraction pattern for monolayer BlueP-Au alloy on Au(111). The electron beam energy was set to be 65 eV.

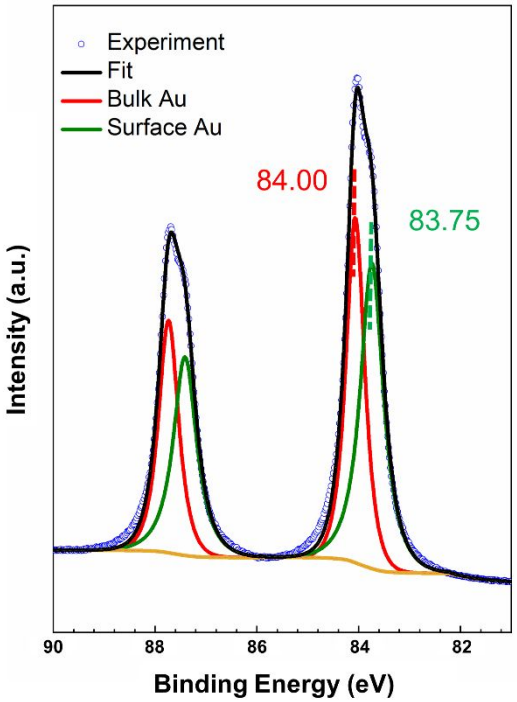

Figure S2. XPS core level spectrum of Au 4f for clean Au(111).

Figure S3 indicates that the P_2Au BlueP-Au alloy features a triangular lattice (marked by green lines) possessing two adjacent potential valleys along each edge, where the potential valleys are marked by the blue hexagons.

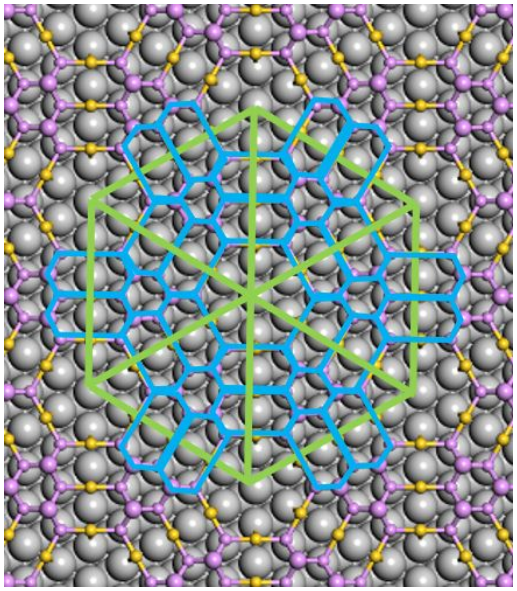

Figure S3. Top view of the optimized atomic structure model for BlueP-Au alloy, which features a triangular lattice.

Figure S4 shows the large scale and close-up STM iamges of depositing potassium onto Au(111) surface at room temperature, where the potassium atoms form into disordered clusters.

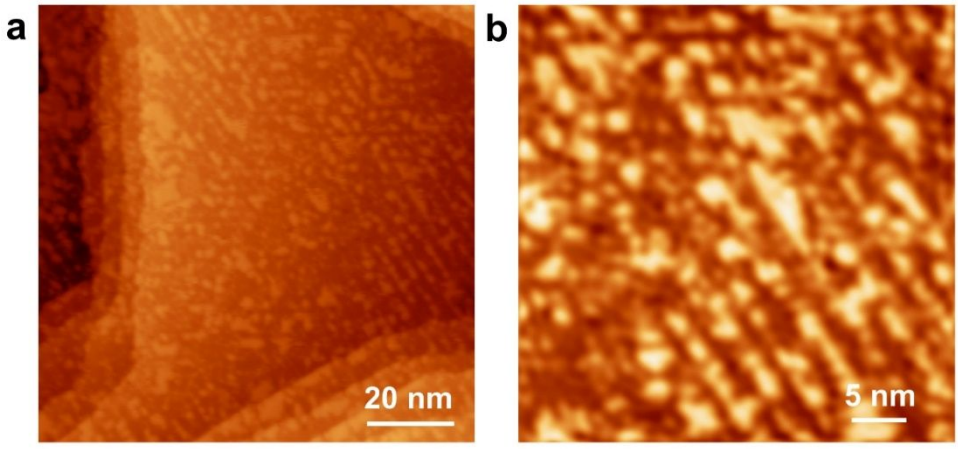

Figure S4. Potassium deposition on Au(111) at room temperature. (a) Large scale and (b) close-up STM images of the disordered potassium clusters on Au(111) after the potassium deposition at room temperature. (V_s = -1.0 V, 100 × 100 nm^2; V_s = -1.0 V, 40 × 40 nm^2).

Figure S5 shows the large scale and the atomically resolved STM images of potassium functionalized Au(111) surface upon room temperature deposition and after post annealing at 500 °C. However, after annealing, potassium atoms cannot be observed in the scanning area, which may be caused by a STM tip-induced diffusion.

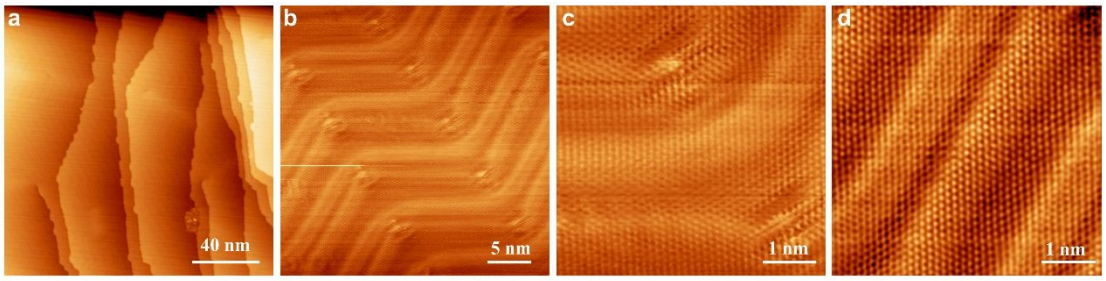

Figure S5. Potassium functionalized Au(111) surface. (a-d) Large scale and atomically resolved STM images of potassium functionalized Au(111) surface. Potassium was deposited onto Au(111) at room temperature followed by post annealing at 500 °C. After annealing, potassium atoms cannot be observed in the scanning area. (V_s = -1.0 V, 200 × 200 nm^2; V_s = -1.0 V, 30 × 30 nm^2; V_s = -1.0 V, 10 × 10 nm^2; V_s = -1.0 V, 10 × 10 nm^2).

Figure S6a reveals the lattice constant of P_2Au alloy is 14.5 Å, which is matched with the 5 × 5 supercell of Au(111). Figure S6b reveals the lattice constant of P_4Au_3 alloy is 11.5 Å, which is matched with the 4 × 4 supercell of Au(111). Notably, there is a seamless connection between these two phases, as shown by the high resolution STM image collected at the domain boundary (Figure S6c and S6d).

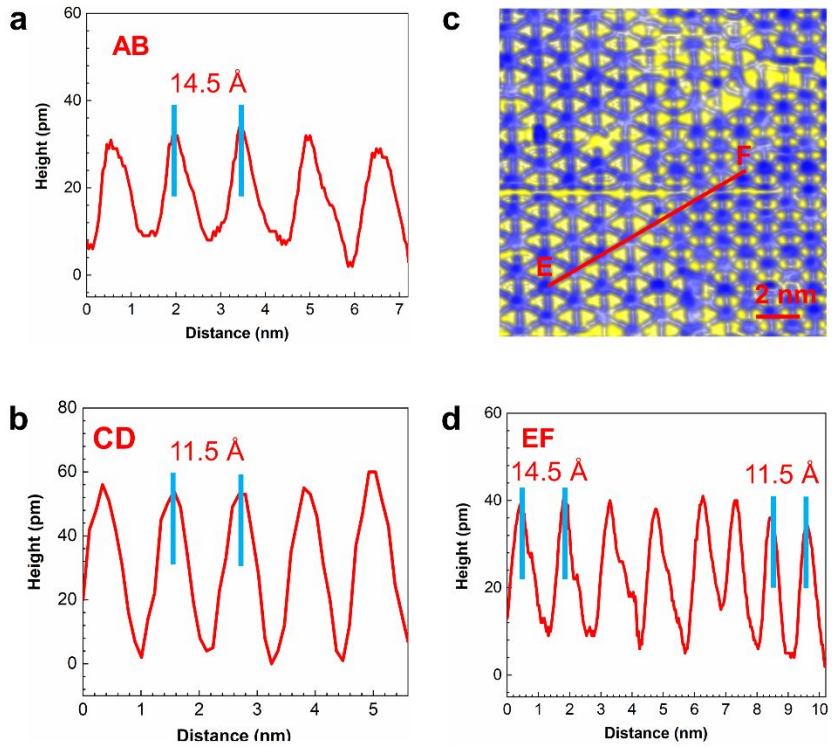

Figure S6. Lattice constants measurements. (a) The section profile along the red line AB in Figure 3b. (b) The section profile along the red line CD in Figure 3c. (c) High-resolution STM image of the boundary between the two phases of BlueP-Au alloys. (V_s = -0.5 V, 15 × 15 nm^2). (d) The section profile along the red line EF in panel c.

Figure S7 is the DFT calculations for the P_4Au_3 BlueP-Au alloy. The new phase P_4Au_3 BlueP-Au surface alloy is matched with the 4 × 4 Au(111) supercell (11.59 Å). Firstly, the two-dimensional (2D) structure composed of P and Au atoms on 4 × 4 Au(111) supercell is also searched by stochastic surface walking (SSW)[1,2] algorithm in the Large-scale Atomistic Simulation with neural network Potential (LASP).[4] An ordered structure is found when adding six Au atoms and eight P atoms on the 4 × 4 Au(111) surface. The phase P_4Au_3 alloy comprises two P_4 clusters and the connecting Au atoms, and the high-buckling P atom in P_4 appears bright in the STM simulation. To check the stability of P_4Au_3 alloy structure, the formation energy is defined as

$$E_{form} = (E_{tot} - E_{sub} - x*E_P - y*E_{Au})/(x + y) \quad (1)$$

where E_{tot}, E_{sub}, E_P, E_{Au} are energies of P_xAu_y (x, y are the number of P and Au atoms) on Au(111), bare Au(111) surface, one P atom in bulk black phosphorus, and one Au atom in bulk Au, respectively. The E_{form} of P_4Au_3 alloy is -0.33 eV, slightly lower than the E_{form} of phase P_2Au alloy structure (-0.40 eV), which indicates the thermodynamic stability of P_4 Au_3 alloy is comparable with that of P_2Au alloy.

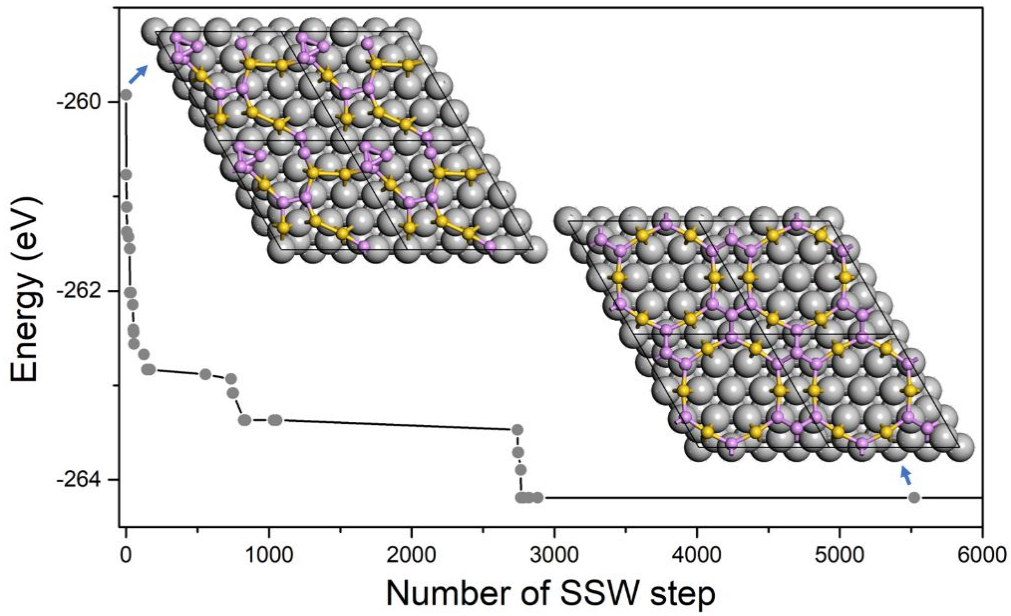

Figure S7. DFT calculations for P_4Au_3 BlueP-Au alloy. Low energy structure evolution of 6 Au atoms and 8 P atoms on 4 × 4 Au(111) during SSW global optimization. Insert are atomic structures of the initial and final stable structures. The phosphorus atoms are

represented by violet. The gold atoms within the alloy are labeled by yellow while the gold atoms of the underlying Au(111) substrate are labeled by gray.

Figures S8c and S8e show the STM images of Kekulé lattice on P_2Au alloy on Au(111) surface with the sample bias held at -0.5 V and -0.02 V, respectively. Each bright dot in Figure S8e can be attributed to one potassium atom adsorbed in the center of the blue hexagon, forming a Kekulé lattice structure. The simulated STM images (Figures S8d and S8f) are in good agreement with the STM observations, and further confirms the validity of our proposed structure model (Figure S8a and Figure 4).

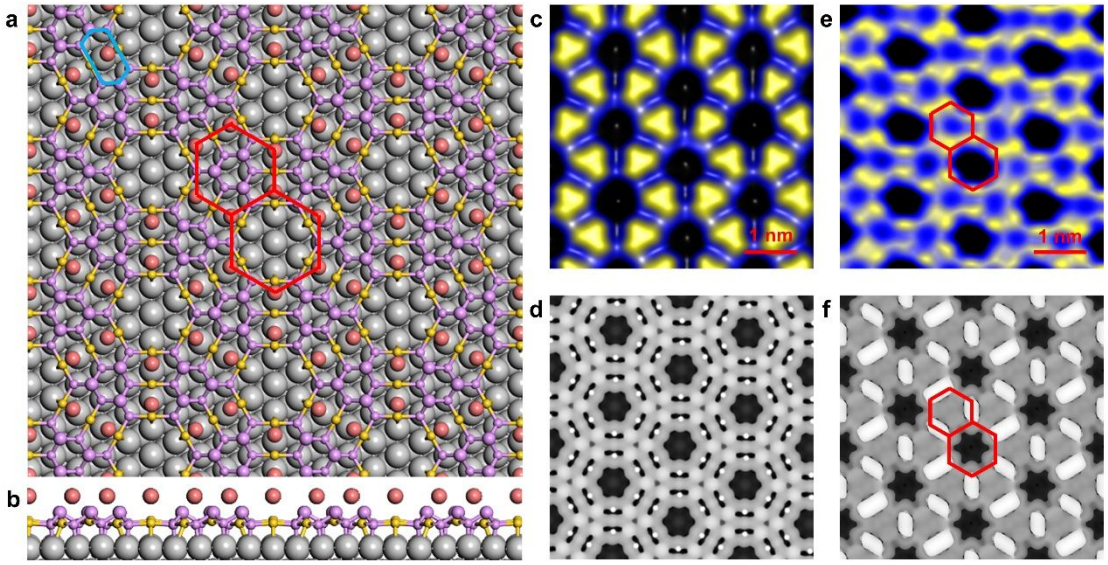

Figure S8. Kekulé lattice on P_2Au alloy on Au(111). (a) Top view and (b) side view of the optimized atomic structure for Kekulé lattice on P_2Au alloy on Au(111) surface. The phosphorus atoms are labeled by violet. The gold atoms of the alloy are labeled by yellow while the gold atoms of the underlying Au(111) substrate are labeled by gray. The potassium atoms are labeled by orange. (c, e) Experimentally observed STM images of the Kekulé lattice on P_2Au alloy on Au(111) at sample bias of -0.5 V and -0.02 V, respectively. (V_s = -0.5 V, 5 × 5 nm^2; V_s = -0.02 V, 5 × 5 nm^2). (d, f) Simulated STM images with bias applied on the sample at -0.5 V and -0.1 V, respectively.

Figure S9 displays the calculated band structure of a Kekulé lattice of potassium atoms on the P_2Au alloy substrate, with gapped Dirac dispersions (~0.25 eV) at Γ point contributed by K atoms.

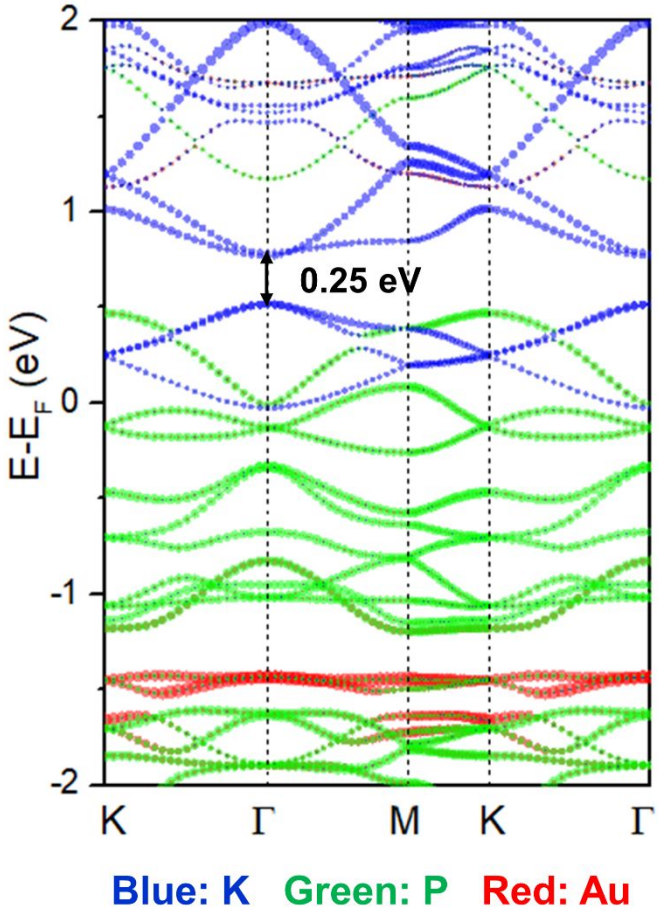

Figure S9. Calculated band structure of a Kekulé lattice of potassium atoms on the P_2Au alloy substrate. High-symmetry k-point paths are sampling along K(1/3, 1/3, 0) →Γ(0, 0, 0) → M(1/2, 0, 0) → K(1/3, 1/3, 0) → Γ(0, 0, 0). The blue, green and red dot lines correspond to the orbitals of K, P and Au atoms, respectively.

In our experiment, the P_4Au_3 phase only appears after K adsorption. Here, we believe the electronic doping of K atoms plays an important role in the P-Au alloy phase transition. To consider the effect of electronic doping, the formation energies of P_2Au and P_4Au_3 phases on Au(111) surface with the same surface doping concentration are calculated, which are shown in Table S1. On bare Au(111) substrate, the E_{form} difference between P_4Au_3 and P_2Au phases is 0.07 eV. When adding the extra electrons on Au(111) substrate, the E_{form} of P_4Au_3 and P_2Au are both decreased, but that of P_2Au decreased faster. When the surface doping concentration is 0.0330 e/Å^2, the E_{form} of P_4Au_3 and P_2Au are almost same, it indicates they have the similar thermodynamic stability.

In addition, to compare the stability of P_4Au_3 and P_2Au structures with K adsorption, the formation energy of $P_xAu_yK_z$ alloy is defined as

$$E_{form} = (E_{tot} - E_{sub} - x*E_P - y*E_{Au} - z*E_K)/(x + y + z) \quad (2)$$

where E_{tot}, E_{sub}, E_P, E_{Au}, E_K are energies of $P_xAu_yK_z$ (x, y, z are the number of P, Au and K atoms) on Au(111), bare Au(111) surface, one atom in bulk black phosphorus, bulk Au, and bulk potassium, respectively. The E_{form} of P_4Au_3 alloy is -0.33 eV, not much less than the E_{form} of P_2Au alloy structure (-0.40 eV). After adsorption of K atoms, E_{form} of $P_8Au_6K_3$ alloy (K adsorption on P_4Au_3 alloy) is -0.61 eV, which larger than that of $P_{18}Au_9K_6$ (K adsorption on P_2Au alloy) phase (-0.53 eV), which indicates the thermodynamic stability of $P_8Au_6K_3$ is comparable with that of $P_{18}Au_9K_6$.

Table S1. The formation energies (E_{form}) of P_4Au_3 and P_2Au phases on the pristine and electron-doped Au(111) substrates under different doping concentrations.

Doping Concentration (e/Å²)	E_{form} **4×4-Au(111)/P_4Au_3 (eV)**	E_{form} **5×5-Au(111)/P_2Au (eV)**	$\Delta E_{form} = E_{4\times4} - E_{5\times5}$
0.0000	-0.332	-0.401	0.069
0.0172	-0.285	-0.320	0.035
0.0258	-0.241	-0.268	0.027
0.0330	-0.207	-0.214	0.007

In experiment, we didn't find the peak of flat band in our STS measurement. Here, we calculated the band structures of a Kagome lattice of potassium atoms on P_4Au_3 alloy with Au(111) substrate (Figure S10a), the feature of flat band (blue dot line) becomes less obvious, where the flat band is immersed in a dispersive band due to the strong substrate interaction. Furthermore, the corresponding projected density of states (DOS) is displayed in Figure S10b, where the DOS contributed by Kagome potassium atoms (blue line) is almost invisible in the Au(111) substrate. This makes it difficult to directly detect the signal of the flat band in the STS measurement.

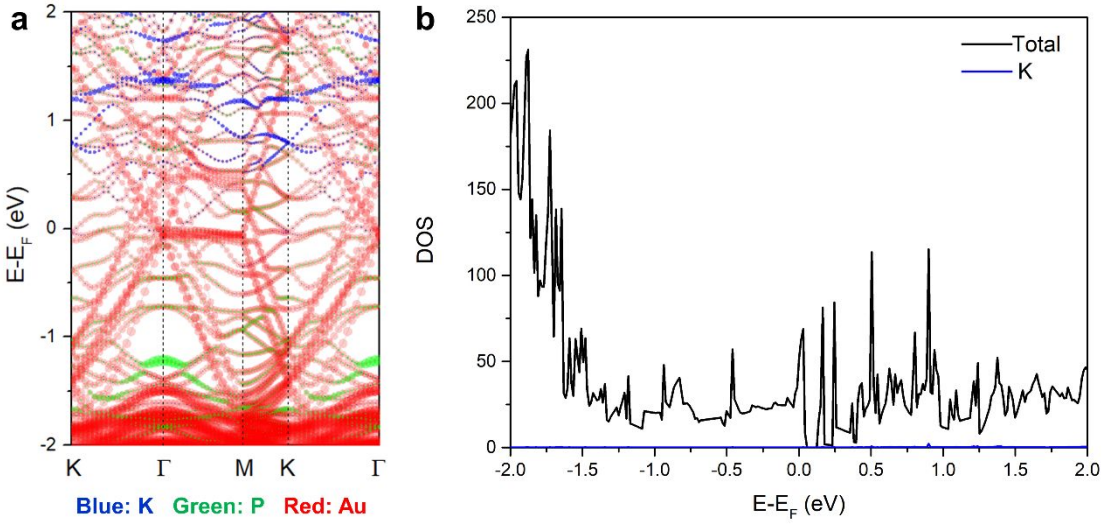

Figure S10. (a) Calculated band structures of a Kagome lattice of potassium atoms on P_4Au_3 alloy with Au(111) substrate. High-symmetry k-point paths are sampling along K(1/3, 1/3, 0) →Γ(0, 0, 0) → M(1/2, 0, 0) → K(1/3, 1/3, 0) → Γ(0, 0, 0). The blue, green and red dot lines correspond to the orbitals of K, P and Au atoms, respectively. (b) The projected DOS. The blue dot line corresponds to the DOS contributed by K.

When potassium distance equals 4.6 Å, which is the equilibrium bond length in bulk potassium, the band structure of the potassium Kagome lattice shows a characteristic of metal bonds (Figure S11a), where the *s* orbitals (blue dotted lines) are mixed with the p_x-p_y orbitals (red dotted lines). At the lattice parameter of 11.6 Å (Figure S11c), the *s* orbitals of the potassium atoms in the Kagome lattice decouple with the p_x-p_y orbitals, and form a flat band. With the increasing of the lattice parameter of the Kagome lattice, the *s* orbitals become more and more localized (Figures S11c-f). Finally, the width of flat band is approaching to zero at the lattice parameter of 16.0 Å. In fact, p_z bands (green dotted lines) of potassium Kagome lattice also show flat band features in Figure S11f, which can be understood as both p_z and *s* orbitals have same symmetry representation and share the same type of hopping.

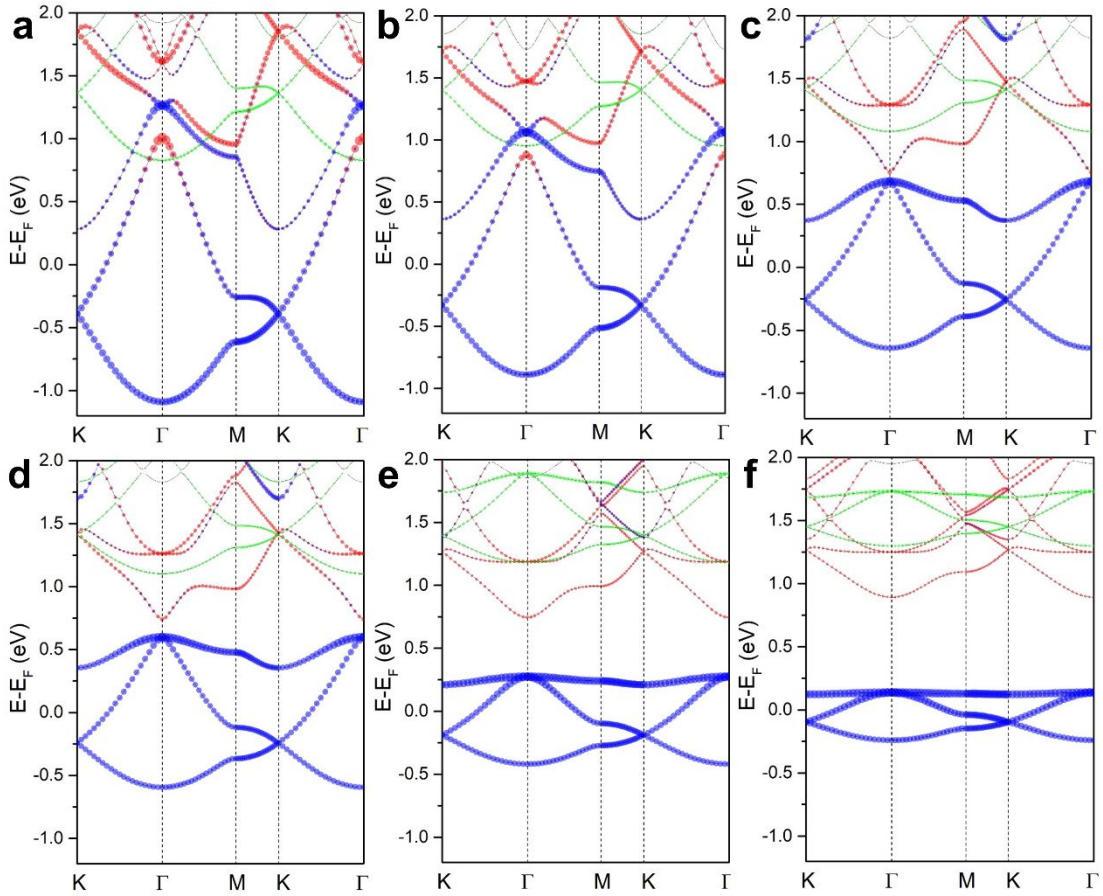

Figure S11. Band structures of Kagome lattice of potassium atoms at different lattice parameters. (a-f) Band structures of Kagome lattice of potassium atoms at the lattice parameters of 9.2 Å, 10.0 Å, 11.6 Å, 12.0 Å, 14.0 Å and 16.00 Å, respectively. The

blue, green and red dotted lines correspond to the s, p_z and p_x-p_y orbitals of potassium atoms, respectively.

References

(1) Shang, C.; Liu, Z.-P. Stochastic Surface Walking Method for Structure Prediction and Pathway Searching. *J. Chem. Theory Comput.* **2013**, *9*, 1838–1845.

(2) Shang, C.; Zhang, X.-J.; Liu, Z.-P. Stochastic Surface Walking Method for Crystal Structure and Phase Transition Pathway Prediction. *Phys. Chem. Chem. Phys.* **2014**, *16*, 17845–17856.

(3) Huang, S.; Shang, C.; Kang, P.; Zhang, X.; Liu, Z. LASP: Fast Global Potential Energy Surface Exploration. *Wiley Interdiscip. Rev. Comput. Mol. Sci.* **2019**, e1415.

(4) Kresse, G.; Furthmüller, J. Efficient Iterative Schemes for *Ab Initio* Total-Energy Calculations Using a Plane-Wave Basis Set. *Phys. Rev. B* **1996**, *54*, 11169–11186.

(5) Blöchl, P. E. Projector Augmented-Wave Method. *Phys. Rev. B* **1994**, *50*, 17953–17979.

(6) Kresse, G.; Joubert, D. From Ultrasoft Pseudopotentials to the Projector Augmented-Wave Method. *Phys. Rev. B* **1999**, *59*, 1758–1775.

(7) Perdew, J. P.; Burke, K.; Ernzerhof, M. Generalized Gradient Approximation Made Simple. *Phys. Rev. Lett.* **1996**, *77*, 3865–3868.

(8) Grimme, S.; Antony, J.; Ehrlich, S.; Krieg, H. A Consistent and Accurate Ab Initio Parametrization of Density Functional Dispersion Correction (DFT-D) for the 94 Elements H-Pu. *J. Chem. Phys.* **2010**, *132*, 154104.

(9) Methfessel, M.; Paxton, A. T. High-Precision Sampling for Brillouin-Zone Integration in Metals. *Phys. Rev. B* **1989**, *40*, 3616–3621.